



PCCP

**A QM:MM Model for the Interaction of DNA Nucleotides with
Carbon Nanotube**

Journal:	<i>Physical Chemistry Chemical Physics</i>
Manuscript ID:	CP-ART-11-2014-005222.R1
Article Type:	Paper
Date Submitted by the Author:	29-Jan-2015
Complete List of Authors:	Chehel Amirani, Morteza; University of Alberta, Mechanical Engineering Tang, Tian; University of Alberta, Mechanical Engineering

SCHOLARONE™
Manuscripts

A QM:MM Model for the Interaction of DNA Nucleotides with Carbon Nanotube

Morteza Chehel Amirani and Tian Tang*

Department of Mechanical Engineering, University of Alberta, Edmonton, AB, Canada

E-mail: tian.tang@ualberta.ca

*To whom correspondence should be addressed

Abstract

Hybrid materials formed by DNA and carbon nanotube (CNT) have shown very interesting properties, but their simulation in solution using quantum mechanical approaches is still a challenge in the computational chemistry community. In this paper, we developed a QM:MM model to study the interactions between charged DNA nucleotides and carbon nanotubes in solution. All four types of DNA nucleotides were taken to interact with two CNTs of similar diameter but different chiralities: (4,4) and (7,0). The nucleotides and CNTs were treated at the QM level, while added water and neutralizing ions were modeled at the MM level. ONIOM simulations were performed at (M06-2X/6-31G(d):Amber) level for the hybrids, as well as for individually solvated CNT and nucleotide, which allowed us to evaluate the energy of binding. Our binding energy values range from 146.60 to 503.43 kJ/mol, indicating strong physisorption of nucleotides on CNTs. The relative large BE, compared with past studies on nucleobase-CNT binding in vacuum, could be due to the larger size of nucleotides compared with nucleobase, the charges on the nucleotides, and the inclusion of solution which causes the release of water molecules upon hybridization.

Keywords: DNA; Nucleotide; Carbon nanotube; QM:MM; ONIOM; Binding energy; DFT

1 Introduction

Since the discovery of carbon nanotube (CNT) in 1991,¹ extensive studies have been performed to uncover its interesting properties. Theoretical and experimental investigations have shown strong dependence of CNT's properties on its structure.² For example, electronic properties of CNT depend strongly on its chirality (n,m) : if $n = m$, the CNT has metallic properties and if $n - m$ is a multiple of 3, the CNT is a semi-conducting material with small band gap.²

Functionalization of CNT has introduced an exciting area of research and various functional groups have been investigated in recent years. DNA is one type of molecule that has exhibited interesting properties when used to functionalize a CNT.³ The intriguing properties of the hybrids formed by DNA and CNT have led to potential applications such as drug delivery,³⁻¹³ biosensing,⁴⁻⁷ CNT dispersion and separation^{8,9} and DNA sequencing.¹⁰⁻¹³ Understanding the process of hybrid formation and the properties of these hybrids are essential to the realization and wide usage of such applications. Theoretically, interaction of DNA polymer with CNT has been widely studied mostly using classical molecular mechanics (MM) simulations. Classical MM approach is suitable to study these large molecular systems, however, it is inaccurate in describing the electronic response of CNT because in those simulations, CNT were completely neutral and only interacted with the DNA through van der Waals (vdW) interactions.¹⁴⁻²¹ Quantum mechanics (QM) approaches can precisely model electronic behavior of materials based on Schrödinger equation. On the other hand, QM approaches are limited to very small systems (typically less than one hundred atoms) due to their high computation cost. Therefore, most QM simulations have been restricted to the interaction of CNT or graphite with small building blocks of DNA including nucleobase, nucleoside or nucleotide. More specifically, binding of individual nucleobases to CNT or graphite constitutes the majority of past studies with QM methods.²²⁻⁴⁰ In addition, most studies using QM methods have been carried out in vacuum while in experiments DNA-CNT hybrids have been formed in an electrolyte solution. Only very few studies considered solution, but in those studies the hybrid structures were still optimized in vacuum, and the solvation energy was simply added using a continuum solvent model. A comprehensive review on the interaction of nucleobases with

graphene or CNT can be found in Chehel Amirani and Tang.⁴¹

While the dominant majority of the past work focused on the interaction of nucleobases with CNT, there are a few works on nucleotide-CNT interactions. Compared with nucleobases, nucleotides are larger molecules that consist of a nucleobase (base), a sugar ring, and a phosphate group. When residing in a solution, the phosphate group in the nucleotide becomes negatively charged and its electric field may be affected if a CNT (electronically responsive) is nearby. Therefore, to resemble the experimental conditions, it is more appropriate to consider the interaction of nucleotide with CNT in solution at the QM level. Wang and Ceulemans employed density functional theory (DFT) with local density approximation (LDA) to study the interaction of adenosine monophosphates with different CNTs in vacuum and evaluated the binding energy (BE) and charge transfer upon hybridization.⁴² In another study also in vacuum, Enyashin et al⁴³ explored the binding between monophosphate nucleotides and a graphene sheet using dispersion-corrected self-consistent-charge density functional based tight binding method (DC-SCC-DFTB) and reported BEs. While attempting to include sugar ring and phosphate group into their simulation, the nucleotides in both works above were kept neutral and no solution was involved. Charged nucleotides were studied by Frischknecht and Martin in an MD work.¹⁴ In their work, the adsorption of nucleotide monophosphates (NMPs) on a (6,0) CNT in solution was studied and BEs were evaluated. Although their model was relatively large, electronic response of the CNT was still lacking. To date, a comprehensive model that takes into account charged nucleotides, solution, and the electronic response of CNT is still missing.

In this study, our goal is to present a more complete model to study the interaction of nucleotides with CNT. Charged nucleotides as well as explicit representation for water and ion are to be considered, which makes our model considerably larger than what has been simulated before at QM level. Since the electronic structure of CNT is important, a proper QM method should be employed to model CNT and nucleotides. The large number of water molecules can be simulated using classical MM approach in order for the simulation time to be manageable. Hence, a hybrid QM:MM model is developed for the nucleotide-CNT interaction. The rest of the paper is

organized as follows. In Section 2, model development and computational details are described. The structural analysis and BE calculations are presented in Section 3. Conclusions are given in Section 4.

2 The QM:MM Model

2.1 Simulated systems

Four DNA nucleotides in the form of monophosphates i.e., nucleoside monophosphate (NMP), were considered in this study: adenosine 5'-monophosphates (AMP), cytidine 5'-monophosphates (CMP), guanosine 5'-monophosphates (GMP) and thymidine 5'-monophosphates (TMP). Figure 1(a)-(d) shows the corresponding molecular structure of the NMPs. It has been reported in a number of experimental and theoretical works that under physiological conditions each of the two singly-bond oxygen atoms carries one negative charge and hence each NMP has a net charge of -2 at neutral pH.^{14,44-49}

Two CNTs were chosen to interact with NMPs: a zigzag CNT with the chirality of (7,0) and an armchair CNT with the chirality of (4,4). These two CNTs have similar diameters (5.48 and 5.42 Å) and hence the effect of their curvature in the binding with NMPs is negligible; however, arrangements of carbon atoms in two CNTs are different. Figure 1(e) and 1(f) shows the molecular structures of the two CNTs. The dangling bonds at the CNT ends were saturated with hydrogen atoms, giving rise to the length of 15.6 Å and 14.8 Å for the (7,0) CNT and (4,4) CNT, respectively. The CNTs lengths are reasonably large to provide a sufficient contact area with NMPs. The numbers of each type of atoms in each structure are listed in Table 1.

NMP-CNT hybrids were assembled by placing the NMPs above the CNT surface. In each system, the nucleobase in the NMP was placed above the CNT surface so that the plane of pyrimidine ring was parallel to a plane defined from a hexagonal ring of carbon atoms on the CNT. Such an orientation was chosen based on previous studies where nucleobases were shown to prefer parallel orientation with respect to the CNT surface in order to maximize the π - π stacking inter-

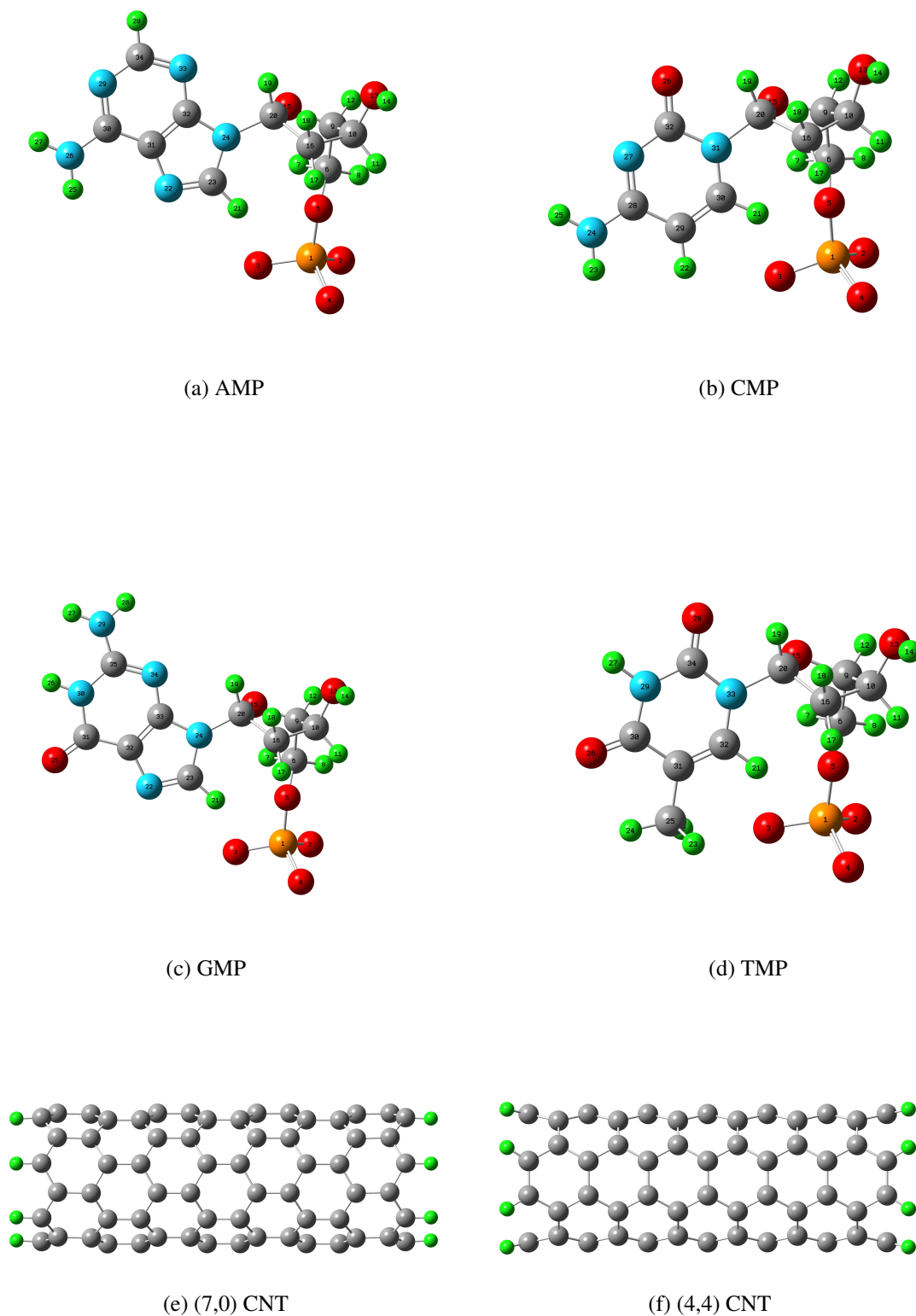


Figure 1: Molecular structures of NMPs and CNTs simulated in this work. Atoms in the NMPs are numbered in (a)-(d) to facilitate later discussion on binding structure.

Table 1: Numbers of each type of atoms in NMPs and CNTs

	C	H	N	O	P
AMP	10	12	5	6	1
CMP	9	12	3	7	1
GMP	10	12	5	7	1
TMP	10	13	2	8	1
(4,4) CNT	104	16	-	-	-
(7,0) CNT	112	14	-	-	-

actions.^{36,38,40,50,51} The separation between NMP and CNT in the initial configuration was set to be 3.2 Å which is close to the optimal distance between nucleobases and CNT reported in previous studies.^{26,28,36,40,52} It is recognized that even with the nucleobase placed parallel to the CNT surface, many initial configurations can be defined, and different initial configurations may result in different optimized structures and BEs. Unfortunately, since our simulated systems are quite large, it is not practical to perform an extensive search to determine the configuration that leads to the most stable structure. Therefore, one initial configuration was chosen for each NMP-CNT system based on our knowledge of what structure might be close to an energy minimum. For the (7,0) CNT, the initial configuration was based on our previous work⁴⁰ where a systematic search was performed to determine the initial configurations that lead to the most stable structures for the corresponding nucleobase-CNT system. For the (4,4) CNT, each NMP was placed above the CNT surface such that the pyrimidine ring in the NMP was aligned with a hexagonal carbon ring on the CNT. The initial configurations for all eight systems are presented in the Supporting Information (Figure S1).

To include the effect of an electrolyte solution, the NMP-CNT hybrids were solvated in explicit water and placed in the center of a box with dimensions of $3 \times 2.4 \times 2 \text{ nm}^3$ generated using Gromacs.^{53,54} Each of the eight systems simulated in this work include 386 water molecules, which makes the density of water in those model systems to be close to the density of bulk water i.e., 1 g/cm³. Due to the net negative charge on NMPs, two Na⁺ cations were added to the solution to

neutralize the system. The location of ions was chosen randomly.

2.2 QM:MM method

QM:MM scheme is a relatively new class of methods in which different regions of a molecular system are modelled using different levels of theory i.e., QM and MM levels. ONIOM (our own n-layered integrated molecular orbital and molecular mechanics) is one of the QM:MM methods which can be used to simulate a molecular system with a reasonable computational cost. In an ONIOM simulation, the molecular system is partitioned into different regions and the energy of the entire system can be expressed as Equation 1 in which "Real" and "Model" refers to the entire system and the QM region, respectively. "High" and "low" refer to the level of theory which are respectively QM and MM.

$$E^{ONIOM} = E^{Model,High} + E^{Real,low} - E^{Model,low} \quad (1)$$

ONIOM method as implemented in Gaussian 09⁵⁵ was used to carry out our simulations. Each system consists of a QM layer and a MM layer. Because there may be charge transfer between the NMP and CNT and this may play important role in their interaction, both entities were considered in the QM region. Due to the large number of water molecules and the unlikely charge transfer with the NMP and CNT, all water molecules and two cations were treated classically in the MM layer. Therefore, there is no covalent bond between QM and MM regions. Figure 2 shows the AMP-(7,0) CNT hybrid in the solution.

To perform the ONIOM simulation, appropriate methods need to be chosen for the MM and QM regions. For the MM calculations, Amber force-field (FF) which is widely used to study the biological systems at atomistic level was employed. It has been shown that Amber FF can be even more accurate than some of the semi-empirical QM methods for such systems.^{56,57} TIP3P model for water molecules was used.

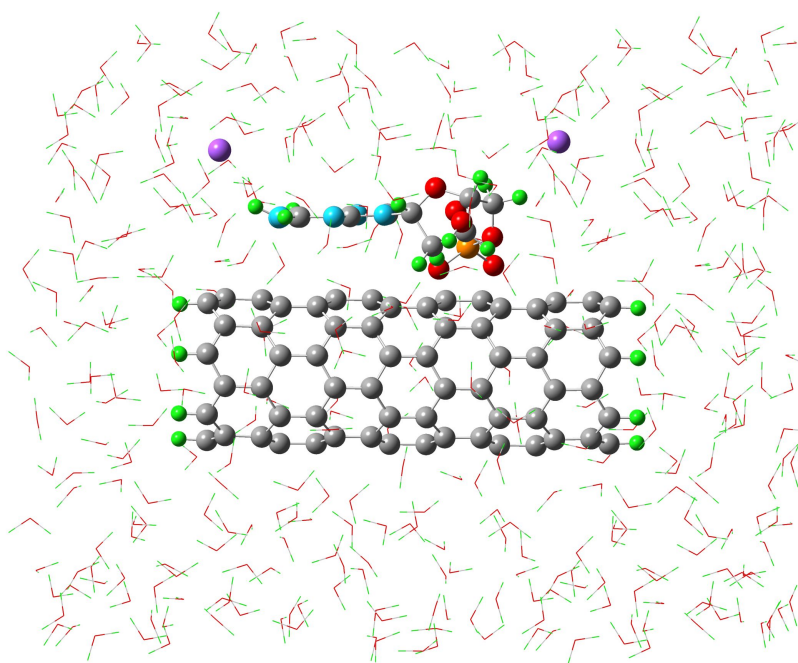


Figure 2: The ONCIOM representation of the solvated AMP-(7,0) CNT hybrid. The two Na^+ ions are colored purple.

For the QM calculation, a wide variety of methods with different levels of complexity and accuracy have been used to study molecular interactions involving nucleobases and nucleotides.^{22–40,42,43,52,58–60} These methods include *ab initio* methods (HF, MP2 and CCSD(T)), DFT and semi-empirical methods, among which DFT has been most widely used due to its relatively low computational cost compared with high level *ab initio* methods and high accuracy compared with semi-empirical methods. It is worth pointing out that dispersion forces, which are universal and among the most important interactions in molecular systems, were poorly treated in many DFT approaches. For the binding of nucleotides to CNT, dispersion can be important in determining the binding structure and BE since it is believed that $\pi - \pi$ stacking plays a crucial role in the binding. A number of dispersion-corrected methods has been proposed.^{57,61–68} Minnesota density functionals (including M05, M05-2X, M06, M06-L, M06-2X, and M06-HF), Grimme's functionals (B97-D, DFT-D2, and DFT-D3),^{69–71} TS,⁷² vdW-DF,⁶² vdW-DF2,⁷³ and B3LYP-DCP⁷⁴ are among the dispersion-corrected methods within DFT that have been used to study $\pi - \pi$ interacting systems. M06-2X functional developed by Truhlar's group has shown good performance in several studies where vdW interaction was important.^{35,52,57,60} To evaluate the suitability of M06-2X functional in modeling our system, we performed a benchmarking study with different basis sets. Individual nucleobases, i.e. adenine (A), cytosine (C), guanine (G), thymine (T) and uracil (U), shown respectively in Figure 3(a) to Figure 3(e), are considered to interact with a benzene ring shown in 3(f). We chose nucleobase-benzene systems for two reasons: first, it is similar to nucleotide-CNT systems in the sense that the interaction is governed by $\pi - \pi$ stacking; and second, results of BE obtained from high level calculations (CCSD(T) method) are available in literature for the nucleobase-benzene system⁵⁷ which allows for the assessment of the M06-2X results.

Configurations for the nucleobase-benzene systems were adopted from the work of Rutledge and Wetmore.⁵⁷ Single-point energy calculations were performed for the individual nucleobases and benzene as well as their hybrids. The BE between nucleobases and benzene is then calculated as follows:

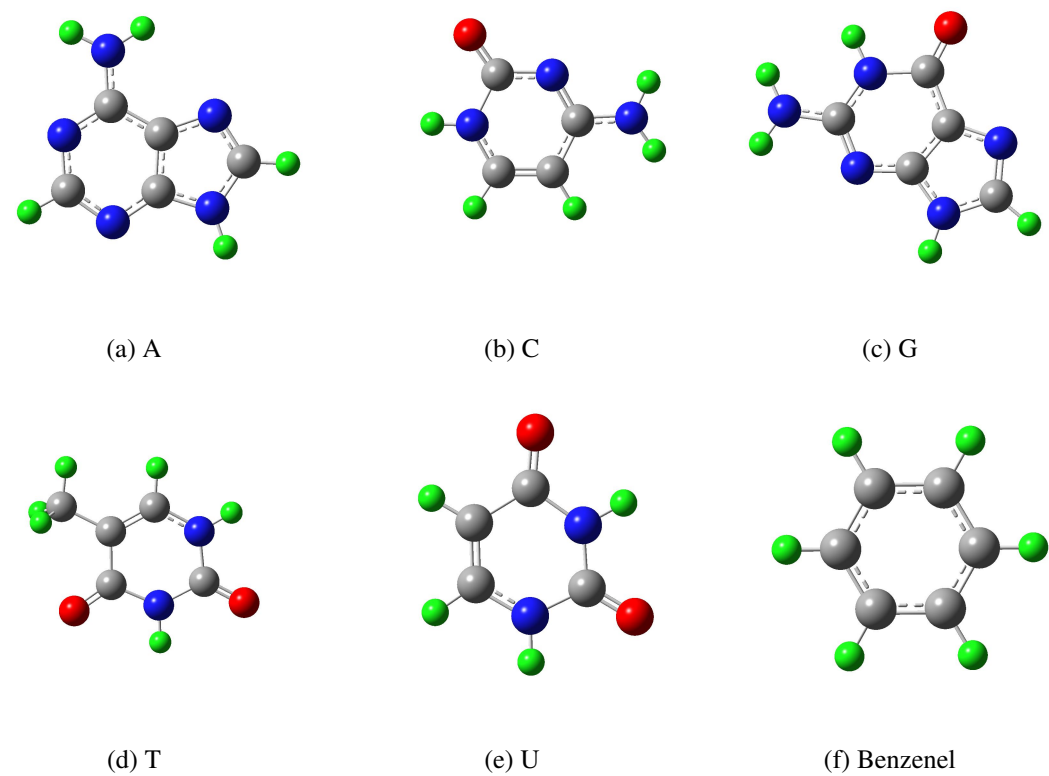


Figure 3: Molecular structures of the nucleobases and benzene for the benchmarking study.

$$BE = |E^{Nucleobase-Benzene} - E^{Nucleobase} - E^{Benzene}| \quad (2)$$

where $E^{Nucleobase-Benzene}$ is the energy of the hybrid, $E^{Nucleobase}$ is the energy of the nucleobase and $E^{Benzene}$ is the energy of the benzene. Several different basis sets were used to test their accuracy. These calculations were conducted using the default fine grid in Gaussian. Since it has been reported that M0-family functionals may have grid size dependency, we examined the effect of grid size by evaluating the BEs at M06-2X/6-31G(d) and M06-2X/6-31+G(d,p) levels using ultra fine grid. Table 2 shows the BE values obtained using M06-2X and the corresponding relative errors (in the parenthesis) compared to the BEs obtained using CCSD(T).

Table 2: BEs (kJ/mol) and relative errors (% in the parenthesis) obtained using M06-2X method compared with CCSD(T)⁵⁷ results

Basis Set	A	G	C	T	U
6-31G(d)	24.8 (6.4)	25.6 (1.2)	20.6 (0.0)	24.6 (0.4)	21.4 (1.0)
6-31G(d) (Ultra fine grid)	24.7 (6.0)	25.6 (1.2)	20.6 (0.0)	24.6 (0.4)	21.5 (0.9)
6-31G(d,p)	24.8 (6.4)	25.7 (1.6)	20.7 (0.5)	24.7 (0.8)	21.5 (0.9)
6-31+G(d,p)	24.4 (4.7)	26.2 (3.6)	21.3 (3.3)	25.0 (2.0)	21.6 (0.5)
6-31+G(d,p) (Ultra fine grid)	24.2 (3.9)	26.2 (3.6)	21.3 (3.3)	25.0 (2.0)	21.6 (0.5)
cc-pVDZ	26.3 (12.9)	27.3 (7.9)	21.5 (4.4)	25.0 (2.0)	21.8 (0.5)

It can be seen that the relative errors are quite small except for A-benzene evaluated using cc-pVDZ. In addition, 6-31G(d) basis set performs well compared with the other basis sets we tested. Our results also show that except for A-benzene and U-benzene systems, grid size has no effect on BEs. Even for those two systems, using ultra fine grid only made a slight difference to the BE. Therefore, to achieve a balance between accuracy and computational efficient, we chose M06-2X/6-31G(d) with fine grid to perform the QM calculation for our NMP-CNT systems.

2.3 Simulation Procedure

All individual NMPs and CNTs were first optimized at M06-2X/6-31G(d) level in vacuum. All atoms were free to relax during this optimization. This step provides appropriate initial structures for the QM:MM simulation in solution. After the optimization in vacuum, Resp charges⁷⁵ were evaluated for each NMP and CNT. This was done by single-point energy calculations at HF/6-31G(d) level using Gaussian, followed by Resp charge calculation using AmberTools.⁷⁶ Partial atomic charges for the two CNTs are presented in Supporting Information (Figure S2). It should be pointed out that the initial atomic charges in the NMPs and CNTs are different from those in the final optimized structures since the NMPs and CNTs were treated at the QM level in the QM:MM simulations.

The individually relaxed NMP and CNT were assembled and solvated to construct the initial configuration for the QM:MM simulation, as described in Section 2.1. Each solvated NMP-CNT hybrids was subjected to a two-step geometry optimization. First, a pure MM optimization was performed in which all atoms were free to move, with the purpose of relaxing atoms specially water molecules and reducing large forces in the system. Amber FF and Resp charges determined from the simulation in vacuum were used in this step. Structure obtained from the MM optimization was then subjected to an ONIOM optimization at M06-2X/6-31G(d):Amber level, where carbon atoms in CNTs were frozen to reduce the computation time.

In order to evaluate the BE between the NMPs and CNTs, two additional simulations were performed, one in which individual CNTs were optimized in water, and the other where individual NMPs were optimized in water in presence of the two ions. The same two-step optimization procedure was followed for these two simulations. The numbers of water molecules in these two simulations were chosen such that they add up to the same as the number of water molecules in the NMP-CNT hybrid simulation (see details below).

2.4 Data analysis

BE between NMP and CNT was calculated for each of the QM:MM model simulated above, according to the following equation:

$$BE = |E^{NMP-CNT} - E^{NMP} - E^{CNT}| \quad (3)$$

where $E^{NMP-CNT}$ is the energy of the optimized hybrid, E^{NMP} is the energy of the relaxed NMPs and E^{CNT} is the energy of the relaxed CNT, all evaluated in presence of solution. Unlike past simulations in vacuum, the BE calculation in the presence of solution is not trivial because of the solute-solvent interactions. In addition, due to the limitations of the ONIOM simulation, applying periodic boundary condition (PBC) was not possible,⁵⁵ and hence free surfaces exist on the periphery of the simulation box. To include the solute-solvent interactions in the calculation of all energy terms in Equation 3, the 386 water molecules in the NMP-CNT hybrid simulation were partitioned into the individual NMP and CNT systems: each CNT was solvated in pure water while each NMP was solvated in water along with the two Na^+ ions.

As pointed out earlier, the lack of PBC introduces free surfaces around the water box, and the surface area of the box in the NMP-CNT hybrid simulation is not equal to the sum of surface areas of the boxes in the individual NMP and CNT simulations. It is well known that water molecules on the surface have different properties compared with the interior ones, due to the different hydrogen bonding network around surface and interior molecules. It has been shown that at room temperature, on average each bulk water molecule forms 3.59 hydrogen bonds,⁷⁷ while each surface water molecule forms ~ 2 hydrogen bonds.^{78,79} One result of this is the high surface tension water possesses. Therefore, the change in surface area can contribute an artificial term in the BE calculated from Equation 3. To correct this, the BE from Equation 3 was modified to eliminate the effect of the free exterior surfaces. Specifically, the changes in surface energy was calculated in Equation 4.

$$\Delta E = |\gamma\Delta S| \quad (4)$$

where γ is the surface tension of water (0.072 N/m⁸⁰) and ΔS is the change in exterior surface area calculated from

$$\Delta S = S^{NMP-CNT} - S^{NMP} - S^{CNT} \quad (5)$$

where $S^{NMP-CNT}$ is the surface area of water box of the optimized hybrid, S^{NMP} and S^{CNT} are respectively the surface areas of the water boxes for the optimized NMPs and CNT. To determine those surface areas, all oxygen atoms of water molecules were used to define a set of points, and a tetrahedral 3 dimensional mesh was created based on those points. The exterior surface of the meshed region was defined to be S and subsequently calculated. The energy correction evaluated in Equation 4 was deducted from the BE calculated in Equation 3 and presented in the results section for the BEs between NMPs and CNT. It should be pointed out upon binding, some water molecules are released from around the solutes into the bulk. As a result, the water surface surrounding the NMP-CNT hybrid also has a different area compared with the total surface area around the individual NMPs and CNTs. However, the energy associated with water release should be considered in the BE, as water release provides one driving force for the binding process. Hence, correction of BE was only performed for water molecules on the outer surface of the simulation boxes.

3 Results

3.1 Structural analysis

Figure 4 shows the optimized structures for the eight systems simulated in this study (with water and ion removed for clarity; images with water and ion are given in Figure S3 of the Supporting Information). In almost all cases (except the GMP-(7,0) CNT system), the nucleobases tend to have parallel orientation with respect to the CNT surface, which was observed in almost all past simulations on nucleobase-CNT binding.^{26,28,38,42,51} Therefore, the presence of phosphate group and sugar ring does not cause strong interruption to the parallel orientation of nucleobases relative to CNT surface, which has also been reported by Wang and Ceulemans in their simulation for the physisorption of DNA nucleoside on zigzag and armchair CNTs.⁴² In Figure 4, the sugar ring in all NMPs exhibits a perpendicular orientation relative to the nucleobase; which was observed in the relaxed NMPs in vacuum and such configuration did not change upon binding to CNT. Overall, little deformation of the internal structure was found during the binding process.

To further explore the location of NMP atoms relative to the CNT, the separation distance between each atom of NMPs and CNT surface in all optimized structures was calculated and shown in Figure 5. In each subfigure, the horizontal axis shows the atom number in the NMP and the vertical axis shows the separation distance of the atoms from the CNT surface. The separation was obtained by first calculating the distance from each atom to the CNT axis and then subtracting from it the radius of the CNT. The two series of data in each plot, presented with different symbols, correspond to the two CNTs. The ranges of the separation distance obtained for AMP, CMP, GMP and TMP adsorbed on the (4,4) CNT are respectively [2.30, 7.66] Å, [2.07, 6.08] Å, [2.09, 7.00] Å, and [2.22, 6.05] Å. The corresponding ranges for the (7,0) CNT are respectively [1.73, 4.95] Å, [1.98, 6.06] Å, [2.12, 5.00] Å, and [1.95, 5.55] Å.

In each NMP, No. 1-5 refer to the atoms in the phosphate group (1: phosphorous; 2 to 5: the four oxygens connected to phosphorous), No. 6 to 20 represent atoms on sugar ring, and the rest of the atoms belong to nucleobases, with the last six being the six atoms in the pyrimidine ring).

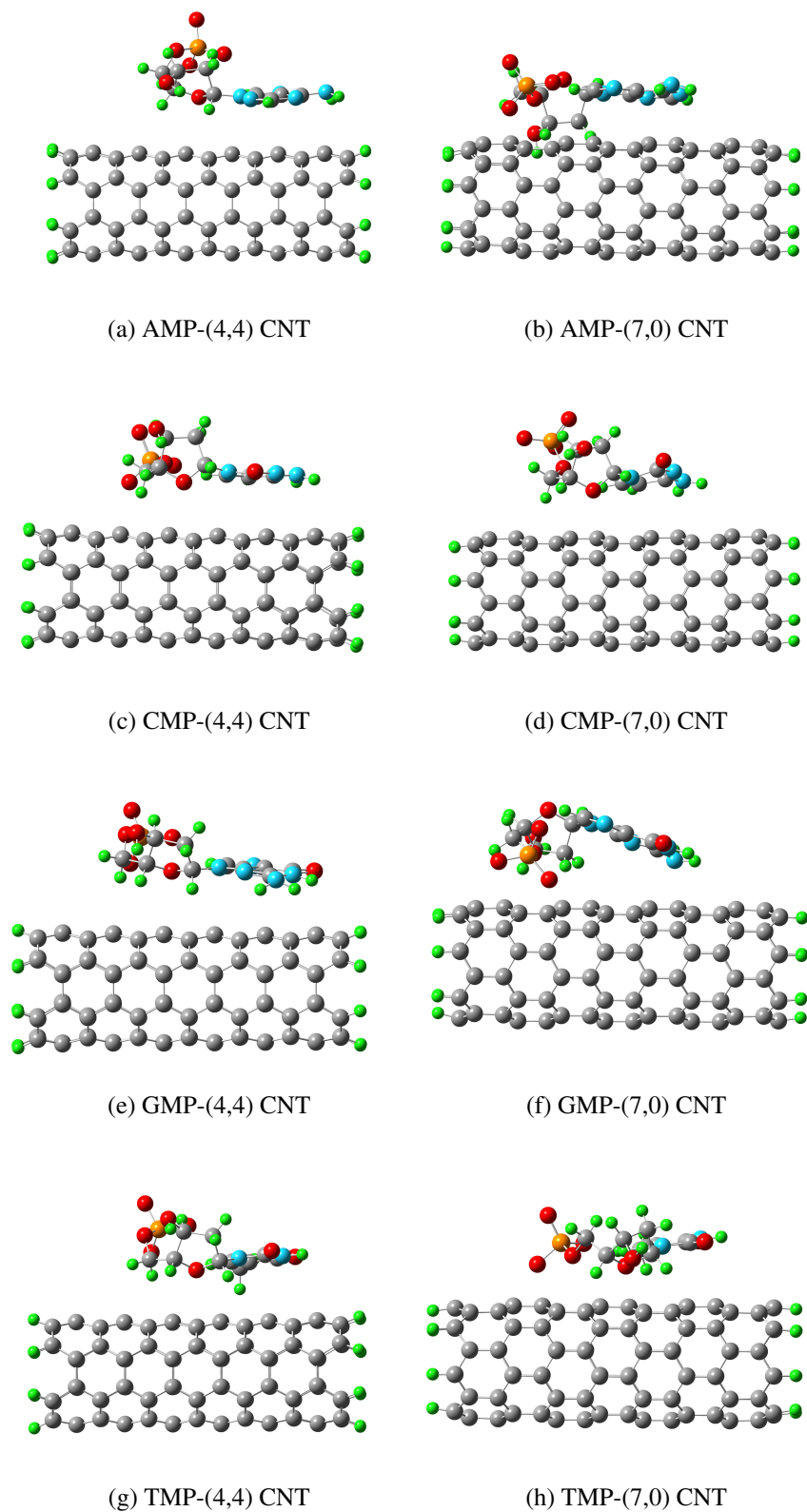


Figure 4: Optimized NMP-CNT structures: (a) AMP-(4,4) CNT, (b) AMP-(7,0) CNT, (c) CMP-(4,4) CNT, (d) CMP-(7,0) CNT, (e) GMP-(4,4) CNT, (f) GMP-(7,0) CNT, (g) TMP-(4,4) CNT, (h) TMP-(7,0) CNT; water molecules and ions are not shown for clarity.

The detailed numbering can be found in Figure 1. It can be seen from Figure 5 that atoms in the phosphate groups are generally located farther from the CNT surface. This is consistent with the hydrophilic properties of phosphate groups in DNA, namely that the DNA backbone tends to expose itself to the solution to maximize contact with water.⁸¹ On the other hand, the six atoms in the pyrimidine ring of NMPs (29-34 in AMP and TMP, 27-32 in CMP, and 30-35 in GMP) are generally located at a distance of ~ 3 Å from the CNT, which confirms the parallel orientation of nucleobases in NMPs relative to the CNT surface.

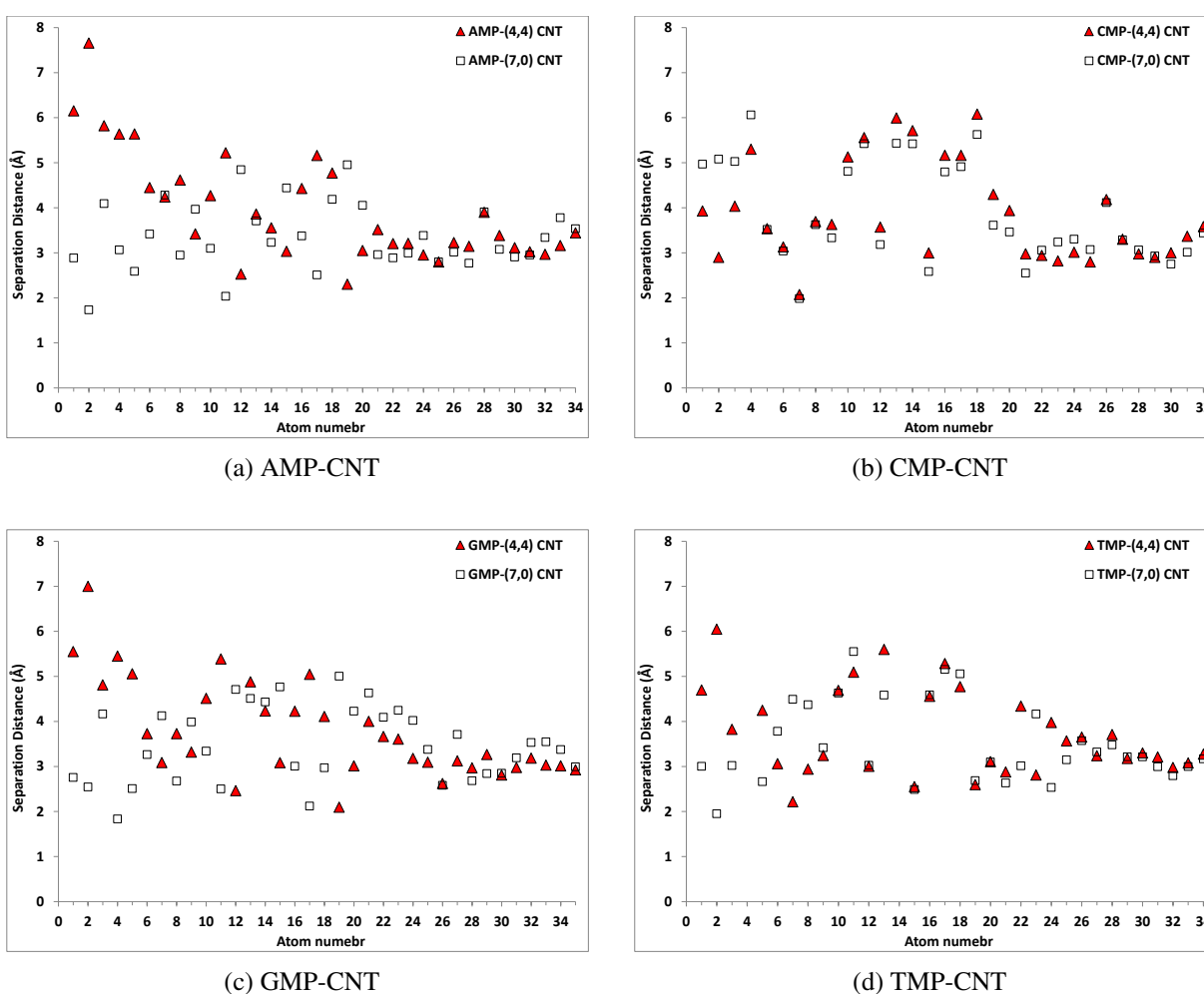


Figure 5: Separation distance between NMP atoms and CNT surface: (a) AMP-CNT, (b) CMP-CNT, (c) GMP-CNT, (d) TMP-CNT; results for NMP-(4,4) CNT and NMP-(7,0) CNT hybrids are respectively indicated by \triangle and \square symbols.

3.2 Binding Energy

BEs between the NMPs and CNTs evaluated based on the method described in Section 2.4 are presented in Table 3. It is recognized that there may be an inaccuracy associated with the calculation of surface area S in Equation 5. Using the initial structure of the NMP-CNT systems as a benchmark, the error was estimated to be around 2-17%. This may result in 2-25 kJ/mol error in the BEs, which is still much smaller than the values of the BE in Table 3 and hence acceptable. The BE values vary from 146.60 to 503.43 kJ/mol, which are relatively larger than past reported energy of binding of nucleobase or nucleotide with CNT or graphene. For the nucleobase-CNT systems, a wide range of BE values covering 5.79 to 115.78 kJ/mol have been reported, depending on the specific system studied and the method chosen to do the optimization and calculation.⁴¹ Compared with the many works on nucleobase-CNT binding, there are only a few studies on the binding of nucleotides with CNT. For instance, the BE between two connected AMPs on CNTs with the chiralities of (7,0) and (4,4) in vacuum was determined to be respectively 337.70 and 303.93 kJ/mol by Wang and Ceulemans.⁴² Given the fact that two connected AMPs were modelled in that work, the BE for a single AMP physisorbed on the CNTs is expected to be around 150-170 kJ/mol, which is comparable to our result for AMP on (4,4) CNT, but smaller than our result for AMP on (7,0) CNT. To the best of our knowledge, the only work on the binding of NMPs with CNT in solution was performed by Frischknecht and Martin, in which the BE was evaluated using molecular dynamics. The BE for a NMP-(6,0) CNT system was determined to vary from 17.99 to 28.87 kJ/mol, depending on the type of NMP and salt concentration, which is considerably smaller compared with our results.¹⁴ Even for the binding of NMPs with graphene which usually possess larger BE compared with CNTs due to larger contact area, smaller BEs (89.73-115.78 kJ/mol) have been reported in vacuum.⁴³

Several reasons might have contributed to the relatively large BEs found in our study. The first is the inclusion of solution and the energy associated with water release. Before binding, the CNT and the NMP are each solvated with certain number of water molecules around it. Upon the physisorption, some water molecules are released into the bulk. As each water molecule form more

Table 3: BE (kJ/mol) between NMP and CNT in solution and contribution of water release (kJ/mol) (in parenthesis)

NMP	(4,4) CNT	(7,0) CNT
AMP	146.60 (27.91)	459.99 (104.58)
CMP	249.13 (163.98)	406.58 (112.81)
GMP	410.96 (118.17)	448.96 (126.46)
TMP	332.43 (153.77)	503.43 (99.87)

hydrogen bonds in the bulk, such water release can contribute to lowering the energy of the system. In fact, water release has been recognized as an important mechanism in the biomolecular binding.^{82–84} Using the same approach employed to evaluate the energy due to change in exterior surface area (See Section 2.4), we estimated the contribution of water release in the BE and presented it in Table 3. Clearly, this contribution is large and is on the order of the BE values. Even though solution was included in some of the previous studies on nucleobase-CNT binding,^{14,17,28,51,85} a continuum model for the solution was typically adopted to estimate the solvation energy, which is probably unable to accurately predict the contribution of water release in the BE.

Secondly, NMPs are charged in this study while all past studies except the work of Frischknecht and Martin¹⁴ studied neutral nucleobases or nucleotides. It has been shown that charged molecules can bind stronger compared with their neutral counterparts.^{86–89} For instance, the adsorption of CO₂, CH₄, and H₂ on Boron Nitride (BN) nanosheets and nanotubes with neutral, 1e⁻, and 2e⁻ charged states was investigated.⁸⁶ The BE between the negatively charged BN nanostructures and the three molecules was reported to be higher compared with the neutral ones, especially for CO₂ molecule. Also, the BE of the hydrogen molecule, H₂, on a doubly charged fullerene, C₆₀²⁺, was shown to be higher than the value for neutral and singly charged fullerenes.^{88,89} In addition, compared with the past works on nucleobase-CNT binding, the presence of sugar ring and phosphate group can considerably enhance the vdW interactions between NMPs and CNT. According to the results for the separation distance in Figure 5, although the phosphate group tends to be solvated in solution, some atoms in the sugar ring and phosphate groups do have similar separation from

the CNT surface compared to the nucleobase atoms. These atoms contribute to the vdW attraction between NMP and CNT, leading to larger BE than nucleobase-CNT binding. As for the work of Frischknecht and Martin, even though the study was performed in solution with the presence of charged NMP and ions, CHARMM force-field was used which could not capture the redistribution of electronic charges upon binding. More importantly, the BE calculation was based on the difference between NMP-CNT energy when they are close and the corresponding energy when the NMP and CNT are separated with a spring force. This force was not excluded from their calculations and might be the source of the relatively low BEs compared with results of Wang and Ceulemans⁴² and our results.

According to the results in Table 3, for the (4,4) CNT the BEs of the four different NMPs follow the order of GMP>TMP>CMP>AMP, while the order for the (7,0) CNT is different, being TMP>AMP>GMP>CMP. Two important factors in determining the order of the BE for $\pi - \pi$ interaction systems are the size and orientation of the molecule. In our study, GMP has the largest size since it contains the highest number of atoms (35) while CMP possess smallest (32). AMP and TMP each contains 34 atoms. The BE results show that GMP has highest BE among the four NMPs for the (4,4) CNT, but it is not the case for the (7,0) CNT. The optimized structure for the GMP-(7,0) CNT (Figure 4(f)) indicates that the nucleobase in GMP is not as parallel as in the other systems which is likely the reason for its smaller BE to the (7,0) CNT compared with TMP and AMP. Although AMP and TMP have the same number of atoms, TMP tends to have higher BE to the CNTs. For the interaction with the (4,4) CNT, the adsorbed TMP is closer to the CNT surface than the adsorbed AMP: the range of separation distance between TMP and the (4,4) CNT is [2.22, 6.05] Å while it is [2.30, 7.66] Å for the AMP. This explains why AMP has smaller BE than TMP and even CMP ([2.07, 6.08] Å from the CNT). For the interaction with the (7,0) CNT, no visible difference in the nucleotide-CNT separation can be observed for AMP and TMP, the cause for the small difference (<10%) in their BE requires further investigation. It is worth mentioning that very different orders for the BE have been reported in the past studies, where the dominant majority focusing on the interaction of nucleobases with CNT in vacuum (See Ref.⁴¹), although G

has been mostly found to bind to CNT more strongly compared with the other nucleobases possibly due to its larger size. For example, Umadevi and Sastry used ONIOM approach at M06-2X:AM1 level to study interactions between nucleobases and armchair CNTs in vacuum.⁶⁰ Atoms in the nucleobases and the "reacting atoms" of CNTs were modeled as the high layer using M06-2X/6-31G(d), although it was not clearly explained what carbon atoms were considered to be reacting. The remaining atoms in CNT were considered as the low layer using semi-empirical AM1. The order of the BE between nucleobases and a (4,4) CNT was determined to be $T > G \sim C > A$, but it changed to $G > T > A > C$ when an additional single-point energy calculation using B3LYP-D method was performed.

Comparing the two different CNTs, BEs for NMP-(7,0) CNT hybrids are in general found to be larger than the ones for the NMP-(4,4) CNT hybrids. This difference shows that two CNTs with very similar diameter and hence similar contact areas may interact differently with the same NMP, due to their different chiralities. Chirality dependence of CNT properties has been previously shown to be important in the dispersion and separation of CNTs.^{8,9} Specifically, in the experiment by Zheng et al.,⁸ it was discovered that single-stranded DNA (ssDNA) can bind to CNT in an aqueous environment and form a hybrid structure where the ssDNA helically wraps around the CNT. The hybrids can be easily dispersed and subsequently separated, using ion exchange chromatograph, according to the chirality of the CNT. In addition, both dispersion and separation of CNTs was found to depend on the sequence of the DNA. Our model showed that different nucleobases and CNT chiralities give rise to different BEs, which may affect the stability of the ssDNA-CNT hybrids in the experiments.

3.3 Limitation and future perspective

The present work is an attempt to more appropriately model the interactions between NMPs and CNT by combining QM and MM approaches. The model has several merits compared with past studies. Firstly, unlike past studies which focused on nucleobase-CNT binding, the current model includes the charged phosphate group and sugar ring, present in real DNA polymer binding with

CNT. Secondly, while past studies usually consider nucleobase-CNT hybrids in vacuum, the current model contains an explicit solution and ions, which does exist in practical applications^{8,9} and can play an important role in the binding. Furthermore, the QM:MM scheme adopted to simulate the binding provides a balance between computational efficiency and accuracy in capturing electronic distribution. In fact, our model contains the largest number of atoms among all available QM and QM:MM simulations on nucleobase/nucleotide-CNT binding. On the other hand, it is important to point out the limitations of this study. First of all, CNTs simulated in this work are short with hydrogen atoms at the two ends. The free edges can introduce some effects on the BE values as well as separation distances. The non-zero partial charges at the edge carbons and hydrogens may also lead to stronger interaction with water compared with infinitely long tube. Application of PBC not only can remove the influence of free edges, but can also more precisely describe electronic properties of CNT. To the best of our knowledge, there is no hybrid QM:MM method available that can include PBC in charged systems. One way to overcome this problem might be using QM approaches with plane wave basis sets in the QM:MM framework. This area of research is being explored to improve the simulation of charged systems using QM:MM methods. Secondly, each geometry optimization in this study was started with a single initial configuration. It has been shown that initial configuration can affect the optimized structures and results of BE.⁴⁰ Performing potential energy scan (PES) and geometry optimization together can be a solution, however it needs more computational time and resources. Furthermore, only neutral pH was considered in the simulations. Different pH value can lead to different deprotonation state of the phosphate group, which can in turn affect the binding. This is an interesting area to be explored in the future. Lastly, only two neutralizing cations were included in our simulations. Different salt concentrations (number of ions) may also affect the results, which was shown by Frischknecht and Martin.¹⁴ It is worth studying the effect of screening ions, which is especially important if one is to better understand how the DNA-CNT interaction changes upon addition of salt under the experimental conditions.⁸

4 Conclusion

A QM:MM model was developed to study the physisorption of nucleotides on CNT surface in solution. The nucleotides and CNTs were modeled at the QM level, while aqueous environment was modelled at the MM level through explicit water molecules and ions. Optimized binding structures were obtained from ONIOM simulations and BEs were calculated from the optimized structures. Our results revealed strong physisorption of nucleotides on CNTs, with the BE in the range of 146.60 to 503.43 kJ/mol for the (4,4) and (7,0) CNTs. The relative large BE, compared with past studies on nucleobase-CNT binding in vacuum, could be due to the larger size of nucleotides compared with nucleobase, the charges on the nucleotides, and the inclusion of solution which causes the release of water molecules upon hybridization.

Acknowledgement

This work was supported by the Natural Science and Engineering Research Council (NSERC) of Canada through the Canada Research Chair program and Discovery Grant. Chehel Amirani acknowledges the support from Sadler Graduate Scholarship in Mechanical Engineering at the University of Alberta. Authors would like to thank WestGrid and Compute/Calcul Canada for providing computing resources and acknowledge Dr. Stacey Wetmore for providing configuration of nucleobase-benzene systems.

References

- (1) Iijima, S. Helical microtubules of graphitic carbon. *Nature* **1991**, *354*, 56–58.
- (2) Saito, R.; Dresselhaus, G.; Dresselhaus, M. *Physical Properties of Carbon Nanotube*; Imperial College Press, 1998.
- (3) Singh, R.; Pantarotto, D.; McCarthy, D.; Chaloin, O.; Hoebeke, J.; Partidos, C. D.; Briand, J.-P.; Prato, M.; Bianco, A.; Kostarelos, K. Binding and Condensation of Plasmid DNA onto

- Functionalized Carbon Nanotubes: Toward the Construction of Nanotube-Based Gene Delivery Vectors. *Journal of the American Chemical Society* **2005**, *127*, 4388–4396.
- (4) Hu, C.; Zhang, Y.; Bao, G.; Zhang, Y.; Liu, M.; Wang, Z. L. DNA Functionalized Single-Walled Carbon Nanotubes for Electrochemical Detection. *The Journal of Physical Chemistry B* **2005**, *109*, 20072–20076.
- (5) Ma, Y.; Ali, S. R.; Dodoo, A. S.; He, H. Enhanced Sensitivity for Biosensors: Multiple Functions of DNA-Wrapped Single-Walled Carbon Nanotubes in Self-Doped Polyaniline Nanocomposites. *The Journal of Physical Chemistry B* **2006**, *110*, 16359–16365, PMID: 16913764.
- (6) He, P.; Bayachou, M. Layer-by-Layer Fabrication and Characterization of DNA-Wrapped Single-Walled Carbon Nanotube Particles. *Langmuir* **2005**, *21*, 6086–6092.
- (7) Xu, Y.; Pehrsson, P. E.; Chen, L.; Zhang, R.; Zhao, W. Double-Stranded DNA Single-Walled Carbon Nanotube Hybrids for Optical Hydrogen Peroxide and Glucose Sensing. *The Journal of Physical Chemistry C* **2007**, *111*, 8638–8643.
- (8) Zheng, M.; Jagota, A.; Semke, E. D.; Diner, B. A.; Mclean, R. S.; Lustig, S. R.; Richardson, R. E.; Tassi, N. G. DNA-assisted dispersion and separation of carbon nanotubes. *Nat Mater* **2003**, *2*, 338–342.
- (9) Zheng, M.; Jagota, A.; Strano, M. S.; Santos, A. P.; Barone, P.; Chou, S. G.; Diner, B. A.; Dresselhaus, M. S.; Mclean, R. S.; Onoa, G. B.; Samsonidze, G. G.; Semke, E. D.; Usrey, M.; Walls, D. J. Structure-Based Carbon Nanotube Sorting by Sequence-Dependent DNA Assembly. *Science* **2003**, *302*, 1545–1548.
- (10) Schneider, G. F.; Kowalczyk, S. W.; Calado, V. E.; Pandraud, G.; Zandbergen, H. W.; Vander-sypen, L. M. K.; Dekker, C. DNA Translocation through Graphene Nanopores. *Nano Letters* **2010**, *10*, 3163–3167.

- (11) Postma, H. W. C. Rapid Sequencing of Individual DNA Molecules in Graphene Nanogaps. *Nano Letters* **2010**, *10*, 420–425, PMID: 20044842.
- (12) Wells, D. B.; Belkin, M.; Comer, J.; Aksimentiev, A. Assessing Graphene Nanopores for Sequencing DNA. *Nano Letters* **2012**, *12*, 4117–4123.
- (13) Merchant, C.; Drndi, M. In *Nanopore-Based Technology*; Gracheva, M. E., Ed.; Methods in Molecular Biology; Humana Press, 2012; Vol. 870; pp 211–226.
- (14) Frischknecht, A. L.; Martin, M. G. Simulation of the Adsorption of Nucleotide Monophosphates on Carbon Nanotubes in Aqueous Solution. *The Journal of Physical Chemistry C* **2008**, *112*, 6271–6278.
- (15) Johnson, R. R.; Johnson, A. T. C.; Klein, M. L. Probing the Structure of DNA-Carbon Nanotube Hybrids with Molecular Dynamics. *Nano Letters* **2008**, *8*, 69–75, PMID: 18069867.
- (16) Johnson, R. R.; Johnson, A. T. C.; Klein, M. L. The Nature of DNA-BaseCarbon-Nanotube Interactions. *Small* **2010**, *6*, 31–34.
- (17) Lv, W. The adsorption of DNA bases on neutral and charged (8, 8) carbon-nanotubes. *Chemical Physics Letters* **2011**, *514*, 311 – 316.
- (18) Manna, A. K.; Pati, S. K. Theoretical understanding of single-stranded DNA assisted dispersion of graphene. *J. Mater. Chem. B* **2013**, *1*, 91–100.
- (19) Mayo, M. L.; Chen, Z. Q.; Kilina, S. V. Computational Studies of Nucleotide Selectivity in DNACarbon Nanotube Hybrids. *The Journal of Physical Chemistry Letters* **2012**, *3*, 2790–2797.
- (20) Neihshal, S.; Periyasamy, G.; Samanta, P. K.; Pati, S. K. Understanding the Binding Mechanism of Various Chiral SWCNTs and ssDNA: A Computational Study. *The Journal of Physical Chemistry B* **2012**, *116*, 14754–14759.

- (21) Xiao, Z.; Wang, X.; Xu, X.; Zhang, H.; Li, Y.; Wang, Y. Base- and Structure-Dependent DNA Dinucleotide/Carbon Nanotube Interactions: Molecular Dynamics Simulations and Thermodynamic Analysis. *The Journal of Physical Chemistry C* **2011**, *115*, 21546–21558.
- (22) Gowtham, S.; Scheicher, R. H.; Ahuja, R.; Pandey, R.; Karna, S. P. Physisorption of nucleobases on graphene: Density-functional calculations. *Phys. Rev. B* **2007**, *76*, 033401.
- (23) Gowtham, S.; Scheicher, R. H.; Pandey, R.; Karna, S. P.; Ahuja, R. First-principles study of physisorption of nucleic acid bases on small-diameter carbon nanotubes. *Nanotechnology* **2008**, *19*, 125701.
- (24) Meng, S.; Maragakis, P.; Papaloukas, C.; Kaxiras, E. DNA Nucleoside Interaction and Identification with Carbon Nanotubes. *Nano Letters* **2007**, *7*, 45–50.
- (25) Meng, S.; Wang, W. L.; Maragakis, P.; Kaxiras, E. Determination of DNA-Base Orientation on Carbon Nanotubes through Directional Optical Absorbance. *Nano Letters* **2007**, *7*, 2312–2316.
- (26) Shtogun, Y. V.; Woods, L. M.; Dovbeshko, G. I. Adsorption of Adenine and Thymine and Their Radicals on Single-Wall Carbon Nanotubes. *The Journal of Physical Chemistry C* **2007**, *111*, 18174–18181.
- (27) Wang, Y.; Bu, Y. Noncovalent Interactions between Cytosine and SWCNT. *The Journal of Physical Chemistry B* **2007**, *111*, 6520–6526, PMID: 17508735.
- (28) Wang, Y. Theoretical Evidence for the Stronger Ability of Thymine to Disperse SWCNT than Cytosine and Adenine: Self-Stacking of DNA Bases vs Their Cross-Stacking with SWCNT. *The Journal of Physical Chemistry C* **2008**, *112*, 14297–14305.
- (29) Ortmann, F.; Schmidt, W. G.; Bechstedt, F. Attracted by Long-Range Electron Correlation: Adenine on Graphite. *Phys. Rev. Lett.* **2005**, *95*, 186101.

- (30) Berland, K.; Chakarova-Käck, S. D.; Cooper, V. R.; Langreth, D. C.; Schröder, E. A van der Waals density functional study of adenine on graphene: single-molecular adsorption and overlayer binding. *Journal of Physics: Condensed Matter* **2011**, *23*, 135001.
- (31) Antony, J.; Grimme, S. Structures and interaction energies of stacked graphene-nucleobase complexes. *Phys. Chem. Chem. Phys.* **2008**, *10*, 2722–2729.
- (32) Panigrahi, S.; Bhattacharya, A.; Banerjee, S.; Bhattacharyya, D. Interaction of Nucleobases with Wrinkled Graphene Surface: Dispersion Corrected DFT and AFM Studies. *The Journal of Physical Chemistry C* **2012**, *116*, 4374–4379.
- (33) Le, D.; Kara, A.; Schröder, E.; Hyldgaard, P.; Rahman, T. S. Physisorption of nucleobases on graphene: a comparative van der Waals study. *Journal of Physics: Condensed Matter* **2012**, *24*, 424210.
- (34) Cho, Y.; Min, S. K.; Yun, J.; Kim, W. Y.; Tkatchenko, A.; Kim, K. S. Noncovalent Interactions of DNA Bases with Naphthalene and Graphene. *Journal of Chemical Theory and Computation* **2013**, *9*, 2090–2096.
- (35) Vovusha, H.; Sanyal, S.; Sanyal, B. Interaction of Nucleobases and Aromatic Amino Acids with Graphene Oxide and Graphene Flakes. *The Journal of Physical Chemistry Letters* **2013**, *4*, 3710–3718.
- (36) Stepanian, S.; Karachevtsev, M.; Glamazda, A.; Karachevtsev, V.; Adamowicz, L. Stacking interaction of cytosine with carbon nanotubes: MP2, DFT and Raman spectroscopy study. *Chemical Physics Letters* **2008**, *459*, 153–158.
- (37) Shukla, M.; Dubey, M.; Zakar, E.; Namburu, R.; Czyznikowska, Z.; Leszczynski, J. Interaction of nucleic acid bases with single-walled carbon nanotube. *Chemical Physics Letters* **2009**, *480*, 269–272.

- (38) Akdim, B.; Pachter, R.; Day, P. N.; Kim, S. S.; Naik, R. R. On modeling biomolecular–surface nonbonded interactions: application to nucleobase adsorption on single-wall carbon nanotube surfaces. *Nanotechnology* **2012**, *23*, 165703.
- (39) Sarmah, A.; Roy, R. K. Understanding the Interaction of Nucleobases with Chiral Semi-conducting Single-Walled Carbon Nanotubes: An Alternative Theoretical Approach Based on Density Functional Reactivity Theory. *The Journal of Physical Chemistry C* **2013**, *117*, 21539–21550.
- (40) Chehel Amirani, M.; Tang, T.; Cuervo, J. Quantum mechanical treatment of binding energy between DNA nucleobases and carbon nanotube: A DFT analysis. *Physica E: Low-dimensional Systems and Nanostructures* **2013**, *54*, 65–71.
- (41) Chehel Amirani, M.; Tang, T. Binding of nucleobases with graphene and carbon nanotube: a review of computational studies. *Journal of Biomolecular Structure and Dynamics* **2014**, 1–31, PMID: 25118044.
- (42) Wang, H.; Ceulemans, A. Physisorption of adenine DNA nucleosides on zigzag and armchair single-walled carbon nanotubes: A first-principles study. *Phys. Rev. B* **2009**, *79*, 195419.
- (43) Enyashin, A. N.; Gemming, S.; Seifert, G. DNA-wrapped carbon nanotubes. *Nanotechnology* **2007**, *18*, 245702.
- (44) Lehninger, A.; Nelson, D.; Cox, M. *Lehninger Principles of Biochemistry*; W. H. Freeman, 2005; Chapter 8.
- (45) Egli, M.; Flavell, A.; Pyle, A. M.; Wilson, W. D.; Haq, S. I.; Luisi, B.; Fisher, J.; Laughton, C.; Allen, S.; Engels, J. In *Nucleic Acids in Chemistry and Biology*; Blackburn, G. M., Gait, M. J., Loakes, D., Williams, D. M., Eds.; The Royal Society of Chemistry, 2006; p 15.

- (46) Ebbing, D.; Gammon, S. *General Chemistry: Media Enhanced Edition*; Cengage Learning, 2007; p 1052.
- (47) Madigan, M.; Clark, D.; Stahl, D.; Martinko, J. *Brock Biology of Microorganisms 13th Edition*; 2010; p 151.
- (48) Wong, A.; Wu, G. Selective Binding of Monovalent Cations to the Stacking G-Quartet Structure Formed by Guanosine 5'-Monophosphate: A Solid-State NMR Study. *Journal of the American Chemical Society* **2003**, *125*, 13895–13905, PMID: 14599230.
- (49) Boghaei, D. M.; Gharagozlou, M. Charge transfer complexes of adenosine-5'-monophosphate and cytidine-5'-monophosphate with water-soluble cobalt(II) Schiff base complexes in aqueous solution. *Spectrochimica Acta Part A: Molecular and Biomolecular Spectroscopy* **2006**, *63*, 139 – 148.
- (50) Varghese, N.; Mogera, U.; Govindaraj, A.; Das, A.; Maiti, P. K.; Sood, A. K.; Rao, C. N. R. Binding of DNA Nucleobases and Nucleosides with Graphene. *ChemPhysChem* **2009**, *10*, 206–210.
- (51) Das, A.; Sood, A.; Maiti, P. K.; Das, M.; Varadarajan, R.; Rao, C. Binding of nucleobases with single-walled carbon nanotubes: Theory and experiment. *Chemical Physics Letters* **2008**, *453*, 266–273.
- (52) Ramraj, A.; Hillier, I. H.; Vincent, M. A.; Burton, N. A. Assessment of approximate quantum chemical methods for calculating the interaction energy of nucleic acid bases with graphene and carbon nanotubes. *Chemical Physics Letters* **2010**, *484*, 295–298.
- (53) Berendsen, H.; van der Spoel, D.; van Drunen, R. GROMACS: A message-passing parallel molecular dynamics implementation. *Computer Physics Communications* **1995**, *91*, 43 – 56.
- (54) Lindahl, E.; Hess, B.; van der Spoel, D. GROMACS 3.0: a package for molecular simulation and trajectory analysis. *Molecular modeling annual* **2001**, *7*, 306–317.

- (55) Frisch, M. J. et al. Gaussian 09 Revision A.1. Gaussian Inc. Wallingford CT 2009.
- (56) Rutledge, L. R.; Durst, H. F.; Wetmore, S. D. Evidence for Stabilization of DNA/RNA Protein Complexes Arising from Nucleobase Amino Acid Stacking and T-Shaped Interactions. *Journal of Chemical Theory and Computation* **2009**, *5*, 1400–1410.
- (57) Rutledge, L. R.; Wetmore, S. D. The assessment of density functionals for DNAprotein stacked and T-shaped complexes. *Canadian Journal of Chemistry* **2010**, *88*, 815–830.
- (58) Chandra Shekar, S.; Swathi, R. S. Stability of Nucleobases and Base Pairs Adsorbed on Graphyne and Graphdiyne. *The Journal of Physical Chemistry C* **2014**, *118*, 4516–4528.
- (59) Lee, J.-H.; Choi, Y.-K.; Kim, H.-J.; Scheicher, R. H.; Cho, J.-H. Physisorption of DNA Nucleobases on h-BN and Graphene: vdW-Corrected DFT Calculations. *The Journal of Physical Chemistry C* **2013**, *117*, 13435–13441.
- (60) Umadevi, D.; Sastry, G. N. Quantum Mechanical Study of Physisorption of Nucleobases on Carbon Materials: Graphene versus Carbon Nanotubes. *The Journal of Physical Chemistry Letters* **2011**, *2*, 1572–1576.
- (61) Johnson, E. R.; Wolkow, R. A.; DiLabio, G. A. Application of 25 density functionals to dispersion-bound homomolecular dimers. *Chemical Physics Letters* **2004**, *394*, 334–338.
- (62) Dion, M.; Rydberg, H.; Schröder, E.; Langreth, D. C.; Lundqvist, B. I. Van der Waals Density Functional for General Geometries. *Phys. Rev. Lett.* **2004**, *92*, 246401.
- (63) Hohenstein, E. G.; Chill, S. T.; Sherrill, C. D. Assessment of the Performance of the M055-2X and M06-2X Exchange-Correlation Functionals for Noncovalent Interactions in Biomolecules. *Journal of Chemical Theory and Computation* **2008**, *4*, 1996–2000.
- (64) Zhao, Y.; Truhlar, D. G. Density Functionals with Broad Applicability in Chemistry. *Accounts of Chemical Research* **2008**, *41*, 157–167, PMID: 18186612.

- (65) Johnson, E. R.; Mackie, I. D.; DiLabio, G. A. Dispersion interactions in density-functional theory. *Journal of Physical Organic Chemistry* **2009**, *22*, 1127–1135.
- (66) Zhao, Y.; Truhlar, D. G. Applications and validations of the Minnesota density functionals. *Chemical Physics Letters* **2011**, *502*, 1–13.
- (67) Grimme, S. Density functional theory with London dispersion corrections. *Wiley Interdisciplinary Reviews: Computational Molecular Science* **2011**, *1*, 211–228.
- (68) Ehrlich, S.; Moellmann, J.; Grimme, S. Dispersion-Corrected Density Functional Theory for Aromatic Interactions in Complex Systems. *Accounts of Chemical Research* **2013**, *46*, 916–926.
- (69) Grimme, S. Semiempirical GGA-type density functional constructed with a long-range dispersion correction. *Journal of Computational Chemistry* **2006**, *27*, 1787–1799.
- (70) Grimme, S.; Antony, J.; Ehrlich, S.; Krieg, H. A consistent and accurate ab initio parametrization of density functional dispersion correction (DFT-D) for the 94 elements H-Pu. *The Journal of Chemical Physics* **2010**, *132*, 154104.
- (71) Grimme, S.; Ehrlich, S.; Goerigk, L. Effect of the damping function in dispersion corrected density functional theory. *Journal of Computational Chemistry* **2011**, *32*, 1456–1465.
- (72) Tkatchenko, A.; Scheffler, M. Accurate Molecular Van Der Waals Interactions from Ground-State Electron Density and Free-Atom Reference Data. *Phys. Rev. Lett.* **2009**, *102*, 073005.
- (73) Lee, K.; Murray, É. D.; Kong, L.; Lundqvist, B. I.; Langreth, D. C. Higher-accuracy van der Waals density functional. *Phys. Rev. B* **2010**, *82*, 081101.
- (74) Torres, E.; DiLabio, G. A. A (Nearly) Universally Applicable Method for Modeling Noncovalent Interactions Using B3LYP. *The Journal of Physical Chemistry Letters* **2012**, *3*, 1738–1744.

- (75) Bayly, C. I.; Cieplak, P.; Cornell, W.; Kollman, P. A. A well-behaved electrostatic potential based method using charge restraints for deriving atomic charges: the RESP model. *The Journal of Physical Chemistry* **1993**, *97*, 10269–10280.
- (76) Case, D. et al. AmberTools12. University of California, San Francisco 2012.
- (77) Jorgensen, W. L.; Madura, J. D. Temperature and size dependence for Monte Carlo simulations of TIP4P water. *Molecular Physics* **1985**, *56*, 1381–1392.
- (78) Raymond, E. A.; Tarbuck, T. L.; Brown, M. G.; Richmond, G. L. Hydrogen-Bonding Interactions at the Vapor/Water Interface Investigated by Vibrational Sum-Frequency Spectroscopy of HOD/H₂O/D₂O Mixtures and Molecular Dynamics Simulations. *The Journal of Physical Chemistry B* **2003**, *107*, 546–556.
- (79) Liu, P.; Harder, E.; Berne, B. J. Hydrogen-Bond Dynamics in the Air-Water Interface. *The Journal of Physical Chemistry B* **2005**, *109*, 2949–2955, PMID: 16851308.
- (80) Vargaftik, N. B.; Volkov, B. N.; Voljak, L. D. International Tables of the Surface Tension of Water. *Journal of Physical and Chemical Reference Data* **1983**, *12*, 817–820.
- (81) Premkumar, T.; Geckeler, K. *Materials Science of DNA*; CRC Press, 2011; pp 77–120, doi:10.1201/b11290-5.
- (82) Ha, J.-H.; Spolar, R. S.; Jr, M. R. Role of the hydrophobic effect in stability of site-specific protein-DNA complexes. *Journal of Molecular Biology* **1989**, *209*, 801 – 816.
- (83) Jayaram, B.; Jain, T. THE ROLE OF WATER IN PROTEIN-DNA RECOGNITION. *Annual Review of Biophysics and Biomolecular Structure* **2004**, *33*, 343–361, PMID: 15139817.
- (84) Jayaram, B.; McConnell, K.; Dixit, S. B.; Das, A.; Beveridge, D. L. Free-energy component analysis of 40 proteinDNA complexes: A consensus view on the thermodynamics of binding at the molecular level. *Journal of Computational Chemistry* **2002**, *23*, 1–14.

- (85) Yamazaki, T.; Fenniri, H. Imaging Carbon Nanotube Interaction with Nucleobases in Water Using the Statistical Mechanical Theory of Molecular Liquids. *The Journal of Physical Chemistry C* **2012**, *116*, 15087–15092.
- (86) Sun, Q.; Li, Z.; Searles, D. J.; Chen, Y.; Lu, G. M.; Du, A. Charge-Controlled Switchable CO₂ Capture on Boron Nitride Nanomaterials. *Journal of the American Chemical Society* **2013**, *135*, 8246–8253, PMID: 23678978.
- (87) Sun, Q.; Wang, M.; Li, Z.; Ma, Y.; Du, A. {CO₂} capture and gas separation on boron carbon nanotubes. *Chemical Physics Letters* **2013**, *575*, 59 – 66.
- (88) Yoon, M.; Yang, S.; Wang, E.; Zhang, Z. Charged Fullerenes as High-Capacity Hydrogen Storage Media. *Nano Letters* **2007**, *7*, 2578–2583, PMID: 17718530.
- (89) Kaiser, A.; Leidlmair, C.; Bartl, P.; Zottl, S.; Denifl, S.; Mauracher, A.; Probst, M.; Scheier, P.; Echt, O. Adsorption of hydrogen on neutral and charged fullerene: Experiment and theory. *The Journal of Chemical Physics* **2013**, *138*, 1–13.